



The gravity and isostatic Moho undulations in Qinghai–Tibet plateau

C. Braitenberg^{a,*}, M. Zadro^a, J. Fang^b, Y. Wang^b, H.T. Hsu^b

^a*Department of Earth Sciences, University of Trieste, Via Weiss 1, 34100 Trieste, Italy*

^b*Institute of Geodesy and Geophysics, Chinese Academy of Sciences, Xu Dong Road 54, 430077 Wuhan, People's Republic of China*

Received 10 May 1999; received in revised form 11 November 1999; accepted 30 December 1999

Abstract

It is our interest to study the Moho depths in the Qinghai–Tibet. An iterative hybrid spectral–classical methodology is applied to invert the gravity data and obtain the 3D variation in Moho depth. The gravity inversion is constrained by results from deep seismic sounding and seismological investigations. The Moho is found between 70 and 75 km depth over most of Tibet. Maximum depths of up to 80 km are found along the margins of the plateau, and shallower depths of 65 km correlate with an important suture running along central Tibet (Bangong Nujiang). At Moho level most of Tibet is isostatically compensated at 90–110%, according to the Airy isostatic model. The Qaidam basin in North-Eastern Tibet and the Tarim basin to the North-West are found to be over-compensated. © 2000 Elsevier Science Ltd. All rights reserved.

1. Introduction

From a geophysical point of view, the Tibet plateau is a region characterized by extremal values: the average topographic elevation of the plateau amounts to 5000 m (Fig. 1). A high seismic activity indicates a highly unstable dynamic situation: between 1901 and 1989 the Tibet plateau was struck by 12 events with $M > 7.0$ and 110 events with $6 < M < 7$ (Zeng and Sun, 1993). The plateau is presently continuing its uplift, as could be confirmed by geodetic

* Corresponding author. Tel.: +39-040-6762258; fax: +39-040-575519.

E-mail address: berg@univ.trieste.it (C. Braitenberg).

measurements. Repeated leveling results (Ma, 1989) have shown that the plateau is rising by an average of 10 mm/year, with a progressive increase from north to south. Repeated relative gravity measurements between Chengdu and Lhasa have been carried out between 1982 and 1992, and have given a relative decrease in Lhasa of 3.6 microgal/year. This result is compatible with the observed uplift rate. (Jiang et al., 1989; Hsu and Jiang, 1995).

In general terms, the uplift of Tibet is connected to the ongoing collision of the Indian and the Eurasian tectonic plates. The convergence rate between India and Southern Tibet has been estimated to amount to 10–25 mm/yr (Jackson and Bilham, 1994; Molnar, 1990). The details of the collision process are presently not well understood, as the relatively inaccessible area makes geophysical investigations difficult.

Geological and geophysical investigations were made during 1982–1987 during the French–English–Chinese cooperation along the 1400 km long Yadong Golmud transect (GGT). The profile extends from the high Himalayas north-eastwards across Tibet (AA' in Fig. 2). Wide-angle fan-profiling provided some insight into crustal structure and Moho depths in Tibet. Detailed description of the southernmost 500 km are given in Hirn et al. (1984). The depth along the remaining part of the profile is reported in Wu et al. (1991a, 1991b) and Xiong Saobo et al. (1985). Beneath most of the Himalayas and Tibet the Moho is found at about 70–75 km depth, along the profile. The Moho depth is characterized by upward steps of up to 20 km in specific sections along the profile. These correlate partly with surface features as the Yarlung Zangbo and the Bangong Nujiang sutures (Fig. 2). Some overlapping segments of crust–mantle reflectors have been interpreted as an indication of the superposition of neighbouring pieces of lower crust along deep thrusts.

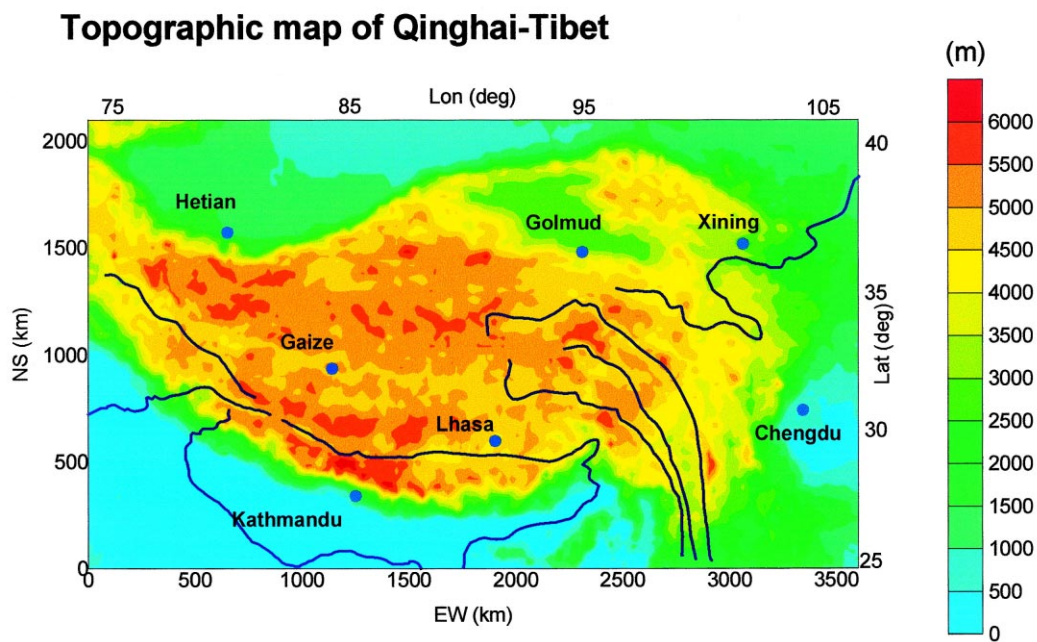


Fig. 1. Topographic map of Tibet–Qinghai, including main towns and rivers.

International cooperation has provided closer insight into the crustal structure in Southern Tibet along 300 km geophysical/geological INDEPTH transect (Nelson et al., 1996), shown in Fig. 2 as the profile BB'. The INDEPTH project built on the previous Sino–French and Sino–British efforts. The project collected near-vertical incidence common-midpoint reflection profiles, wide-angle reflection data, broad band earthquake, magnetotelluric and surface geological data. The Moho was reached in the southern part of the transect at 75 km depth by active seismic sounding. In the northern part a reflection horizon at 15–20 km prevented the Moho to be seen. The reflection was ascribed to the presence of partially molten crust. In favor of this hypothesis was a low-velocity crustal zone observed by receiver functions (Kind et al., 1996) and a high-conductivity layer in the magnetotelluric (MT) profile (Chen et al., 1996). The Moho in this part could only be found by broad band earthquake recordings at depths between 70 and 80 km (Brown et al., 1996; Nelson et al., 1996). The deep seismic sounding revealed evidence of an active thrust fault along which the Indian plate is underthrusting Southern Tibet. The thrust fault, named MHT (Main Himalaya Thrust) dips north at an angle of about 9° and has been observed at depths between 30 and 40 km at latitudes between 27° and 29° N. It is not shown in Fig. 2, as its link to the thrust faults observed at the surface is still unclear. The MHT extends at least 200 km north of the Himalayan thrust front or MBT (Main Boundary Thrust) (Zhao Wenjin et al., 1993; Nelson et al., 1996).

Gravity and topography data of Tibet have been studied jointly in Jin Yu et al. (1994) by evaluation of the statistical and spectral properties of the fields. The cross correlation analysis of gravity anomalies and topography along three profiles orthogonal to the Himalayan arch made at higher frequencies suggests positive correlation at wavelengths of 150 km and negative correlation at 500 km, which has been interpreted as the folding of Tibet (Jin Yu et al., 1994).

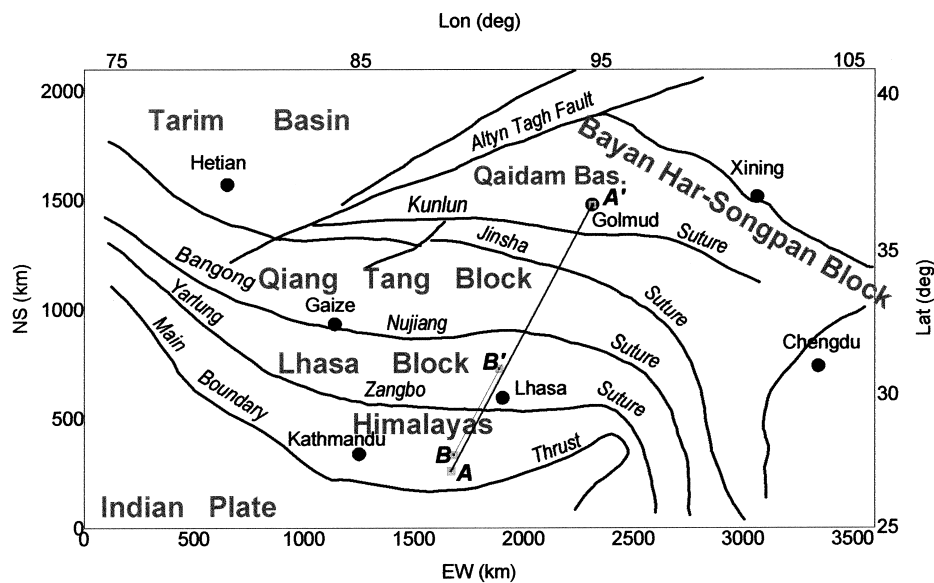


Fig. 2. Main tectonic lines and units in Tibet area (Meng Lingshun et al., 1992). The line AA' marks the Yadong Golmud profile (Wu et al., 1991a), the BB' the INDEPTH profile (Nelson et al., 1996).

The coherence is modeled as that of a rheologically layered plate with a mid-crustal discontinuity (Conrad) at 13 km, and the Moho set at 60 km. The lower crust is assumed to be ductile and less rigid than the upper crust and upper mantle.

In a successive paper Jin Yu et al. (1996) study the Bouguer anomalies along six profiles crossing Tibet. They use a model of two plates of variable elastic thickness, the Indian and the Eurasian plates, subducting the Tibetan crust. The Indian plate has elastic thickness of 90 km, weakening below the Himalayas. The Eurasian lithosphere has a lower elastic thickness of 40 km. The long wavelength Bouguer anomalies are explained by a thickened crust approximately obeying the linear depth/topography relationship predicted by the Airy isostatic model and the effect of the subducting lithosphere. In the central part of Tibet some relief on the Moho is introduced which is ascribed to the bending moment on the subducting plates, generated by shear stress along the mantle suture.

The evaluation of admittance and coherence functions of topography and Bouguer gravity anomalies over the Himalayan area brought Wang and Hsu (1996) to the conclusion that the surface and subsurface loads are supported by both the strength of the lithosphere and the local compensation. The effective elastic thickness of the Tibet plateau was found to be 80–90 km.

The questions remained open following the above gravimetric studies are first to give a full 3D model of the Moho underlying Tibet and its gravity effect, an improvement with respect to the models along profiles. Secondly, all available material on crustal and lithospheric structure shall be used in the model. In the present study, we pursue such a task performing a 3D inversion of the gravity field over the entire Tibet plateau. The inversion is made taking into account the Bouguer gravity data, the results of the INDEPTH crustal investigations, and of the GGT Yadong Golmud transect. We use the results from the deep seismic refraction studies (DSS) in order to constrain the inversion. In the ideal case, a gravimetric study sets the goal of modeling the entire crust, and if possible also part of the upper mantle with appropriate density values. For the Tibet area though, these expectations must be reduced, due to the scarce constraints available. The approach we use aims at limiting the model to the Moho undulations, which are responsible for the longer wavelength gravity variations. In the future, when more DSS lines will be available, it can be thought of modeling the crust as a whole.

It is interesting to compare the Moho obtained from gravity inversion with that predicted by an isostatic model. From the deviations of the two quantities some conclusions on the geodynamics can be drawn. If the isostatic Moho is coincident with the Moho obtained from gravity inversion, it means that the crust is in isostatic equilibrium, and that the buoyancy forces cannot be made responsible for the uplift. An example for which the crust is deeper than expected from the isostatic hypothesis is given by the South-Eastern Alps, where the discrepancy amounts to about 10 km (Braitenberg et al., 1997).

2. Geological outline

A complicated structural collage consisting of various microplates (terranes) split from the Gondwanaland and Eurasian plate characterizes the Qinghai–Tibet plateau (e.g. Chengfa et al., 1986). It is composed (Fig. 2) of the Kunlun/Bayan-Har-Songpan, Qiang-Tang, Lhasa and Himalayan microplates with four major suture zones between one another. It is generally

accepted that the plateau has undergone a history of multiple collisions. Multiple collisions in different geological epochs have produced successively the Kunlun, Jinsha, Bangong Nuijiang and Yarlung Zangbo suture lines. The tectonic evolution of the Qinghai–Tibet plateau in the Mesozoic is actually the history of the splitting of the northern margin of the Gondwanaland, which may have been formed as a single platform during the late Paleozoic to early Mesozoic, and the history of its subsequent collision with the Eurasian plate. For the late Precambrian and Paleozoic, there is evidence of accretion of the continental sea of the Gondwanaland and Eurasian passive continent. In the Mesozoic, the northern margin of the Gondwanaland was disintegrated and drifted; the Meso-Tethys was developed and subsequently closed, and the microplates within the Meso-Tethys finally collided with each other. In the Cenozoic, the shortening, doubling and uplifting of the crust characterized the whole plateau. The main characteristics of its tectonics and crust–mantle structure are as follows: the plateau itself consists of several zones of comparatively high plasticity, surrounded by several large rigid masses. The tectonic lines run nearly E–W. Several large left lateral strike-slip faults, such as the Altyn Tagh, the Kunlun, the Xianshuihe, are predominant in the north and eastern part of the plateau. Further west, the lines form a tight fold zone of Pamirs, while to the east they turn rapidly to form the S–N tectonic belts. The tectonic belts formed by N–S compression are dominant in the central part of the plateau, while shear zones dominate in the eastern and western segments, forming a series of dextral strike-slip faults.

3. Methodology used in the gravity inversion

The methodology applied in the gravity inversion is an iterative hybrid spectral–classical inversion method. It has been introduced and extensively tested in 2.5D applications in Braitenberg et al. (1997) and used in Braitenberg and Drigo (1998). A first application to 2D gravity surveys was done for the South-Eastern Alps, where the 3D Moho undulations were investigated, giving excellent agreement with the Moho depths found by seismic methods (Zadro and Braitenberg, 1997). A discussion of a synthetic case of 3D modeling was discussed in Braitenberg and Zadro (1999).

A boundary with fixed density contrast ($\delta\rho$), separating two horizontal layers, is assumed to be set at the depth (d). The undulations $h(x,y)$ of the boundary are to be determined by gravity inversion of the observed gravity field. The observed gravity field must be corrected for contributions of density inhomogeneities lying above or below the boundary. Assuming the discontinuity to be studied being the crust–mantle boundary (Moho), a lower frequency contribution may arise from lithospheric thickening. Mid-crustal to superficial inhomogeneities affect increasingly higher frequency bands of the gravity observations, and may be separated by filtering processes. In the ideal case that a density model of the mid- to superficial part of the crust can be made, it is preferable to eliminate these gravity contributions by direct evaluation. In the case that insufficient information is present for complete modeling, one must rely on the statistical method, which bases on the spectral properties of the gravity potential field.

Supposing the part of the gravity field related to the boundary undulation being $g_0(x,y)$, sampled on a regular grid $n = 1, N$; $m = 1, M$, with sampling δx , δy , the Fourier Transform

(FT) is computed, obtaining the 2D spectrum $F_0(n,m)$. In the first iteration step, the undulation of the boundary is obtained from downward continuation:

$$h_1(n,m) = \text{FT}^{-1} \left[F_0(n,m) e^{sd} \frac{1}{2\pi G} \delta\rho \right]$$

$$s = \sqrt{\left(\frac{n}{N\delta x} \right)^2 + \left(\frac{m}{M\delta y} \right)^2} \quad (1)$$

The undulation of the boundary is approximated by a series of rectangular prisms of sides a and b and density $+\delta\rho$ or $-\delta\rho$, according to whether the boundary is above or below the reference level (d), respectively. The gravity field $g_1(n,m)$ obtained from the direct computation (Nagy, 1966) is used for calculating the gravity residual $\delta g_1(n,m) = g_1(n,m) - g_0(n,m)$. The FT of the gravity residual is substituted for the gravity field in Eq. (1), in which by means of the downward continuation, a correction to the boundary undulation is obtained. The iterations are repeated following this scheme, obtaining a successively decreasing correction to the undulation, or, equivalently, a decreasing root mean square (rms) gravity residual. That the iterations are always necessary is due to the fact that Eq. (1) is only an approximation to the relation between the FT of the gravity field and the FT of the undulation of the boundary. As can be seen from the series expansion of Parker (1972) the above relation uses only the first term of the series. In all synthetic test situations the iterations converged, and a unique solution to the boundary undulation was retrieved, if the correct values of density contrast and reference depth were given in input. For more details we refer to the above mentioned papers.

At every iteration step a low pass filtering of the gravity field is applied in order to limit the maximum spatial frequency of analysis, depending on the depth of the boundary (d). This takes care of the fact that the Moho undulations are not related to the high frequency part of the gravity field, caused by masses located above the discontinuity layer. The limitation in frequency overcomes also the problem that the downward continuation becomes unstable at high frequencies. We use a circularly symmetric modified Hamming frequency filter defined by the following expression, (s) being the spatial frequency (Eq. (1)), and p_{\min} the cut-off wavelength:

$$\begin{aligned} H(s) &= 0.5(1 + \cos(2\pi s p_{\min})) & s \leq 1/p_{\min} \\ H(s) &= 0 & s > 1/p_{\min} \end{aligned} \quad (2)$$

4. Gravity inversion

The gravity inversion is carried out on the geographic window (longitude 75–105°, latitude 25–41°) centered on the Tibet plateau. The gravity data used are 10' × 10' gridded Bouguer anomalies. Resources were based on the Chinese gravity network 85, with height reference the Yellow Sea (Sun, 1989). The gravity data were reduced using the Helmert gravity formula. A complete terrain correction was made using a topographic density of $2.67 \times 10^3 \text{ kg/m}^3$. The

overall data error in the Bouguer values is estimated to be 1 mgal. The missing gravity data south of the Himalayan arch were substituted with Bouguer gravity values derived from the IGG97L (Institute of Geodesy and Geophysics, CAS, Wuhan) Earth gravity model (Hsu and Lu Yang, 1995; Lu Yang and Houze, 1998), complete to degree and order 720 in China and available on a $30' \times 30'$ grid. At last the data have been interpolated on a regular grid of 20 km \times 20 km, the grid extending 2540 km in N–S and 3900 km in E–W direction. The data grid exceeds the area to be studied by 110 km on all sides, in order to allow for a buffer zone reducing border effects. The results of the gravity inversion are limited to the area for which the densely spaced data are available. In Fig. 3 the Bouguer anomaly map is shown, and the region excluded from the discussion is identified as the hatched area. The main tectonic lines and the locations of principal towns have been added to the map for better orientation.

At first the observed gravity data are corrected for the lithospheric thickening. The lithosphere thickening obtained from seismic investigations and available on a $2^\circ \times 2^\circ$ grid (Zhou et al., 1991), is approximated by rectangular prisms of 220 km \times 220 km sides. The density contrast of lithosphere to asthenosphere is set equal to $0.04 \times 10^3 \text{ kg/m}^3$ and the depth of the equilibrium boundary is set to $d = 90 \text{ km}$, following the investigations of Zhou et al. (1991). The lithosphere thickness model is shown in Fig. 4 and the gravity effect is given in Fig. 5, this last amounting to a correction ranging from -16 to 60 mgal. The effect of a thick lithosphere beneath the Tibet plateau leads to a uniform positive gravity effect of between 40 and 60 mgal for most of the area. This value compares well with the lithosphere gravity effect of the flexure model found by Jin Yu et al. (1996), who find a positive effect of about 50 mgal along the profiles crossing Tibet. To the east of Tibet, the gravity correction is small and is

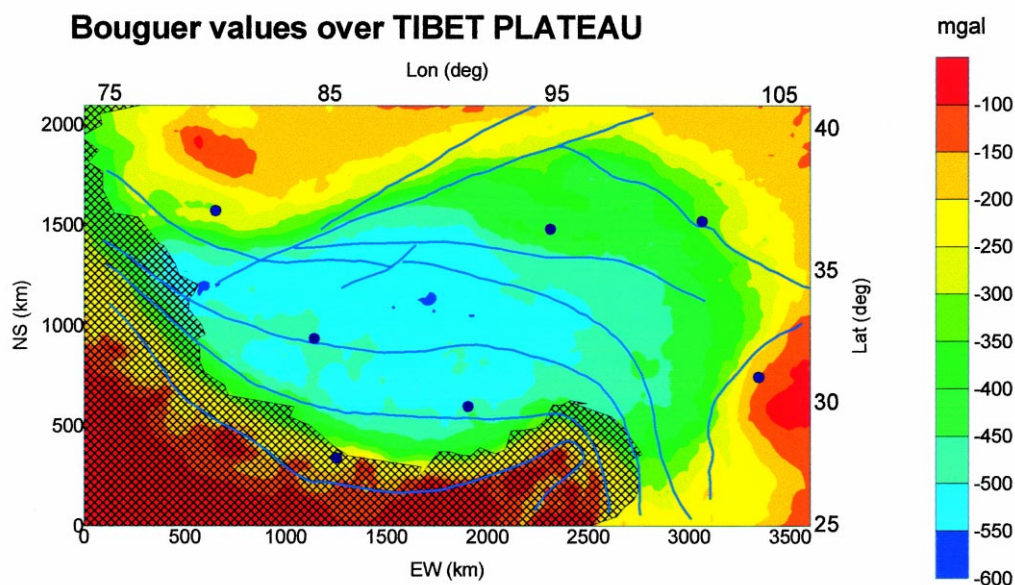


Fig. 3. Bouguer anomaly map with tectonic lines. The hatched area marks the region not covered by the Chinese gravity database.

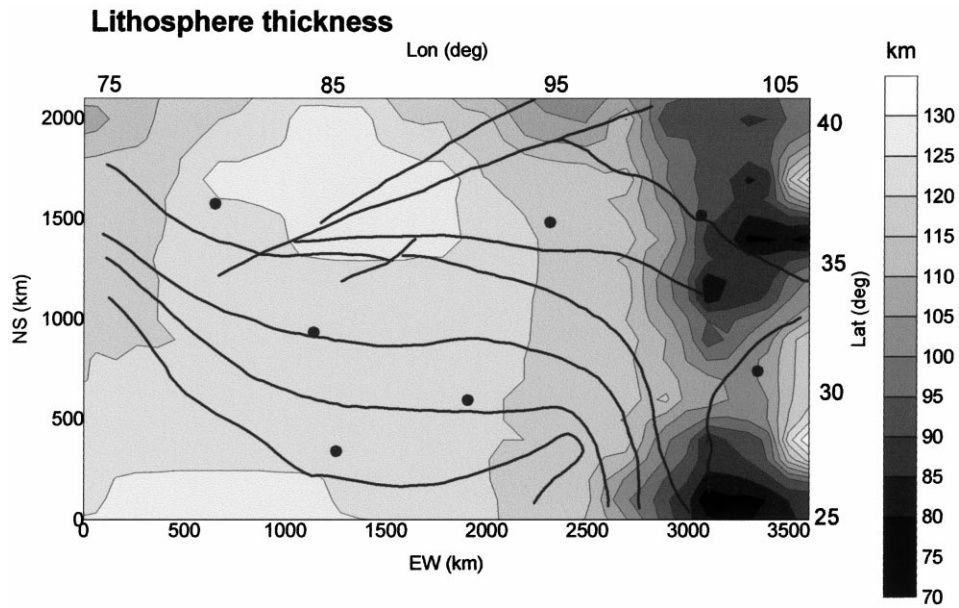


Fig. 4. Lithospheric thickness model of Zhou et al. (1991) with tectonic lines.

mostly below 15 mgal. The main tectonic lines have been added to the map for better orientation.

The gravity data, corrected for the lithosphere effect are low-pass filtered with the modified Hamming filter, with cut-off wavelength $P_{\min} = 200$ km. The cut-off wavelength of 200 km

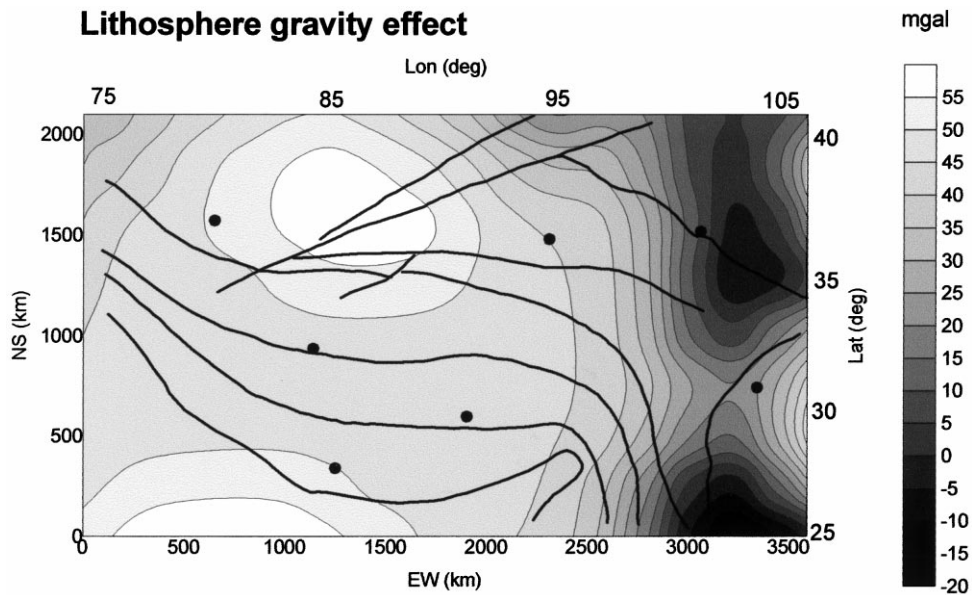


Fig. 5. Gravity effect of lithospheric thickening and main tectonic lines. The lithosphere model is shown in Fig. 4.

eliminates the part of the gravity field which is generated in the mid- or upper crust. In fact the investigations of Jin Yu et al. (1994) showed that the gravity variations of wavelengths longer than 150–200 km are likely due to the masses seated at depths of 50–100 km, which corresponds to the Moho level. The side length of the square prism used for calculating the gravity effect of the undulating boundary is chosen to be 260 km. The number of iterations is fixed to four. Fixing the number of iterations does not alter the results obtained, as will be shown later.

The inversion procedure necessitates a-priori values for the reference depth (d) and the density contrast ($\delta\rho$) across the Moho boundary. This can be made by using generally accepted mean values as $d = 30\text{--}35$ km and $\delta\rho = 0.3\text{--}0.5 \times 10^3$ kg/m³, and defining the resultant Moho within the subsequent uncertainty boundaries. Alternatively, different couples of geophysically plausible density and depth values can be tested and the seismic Moho, where available, be used as boundary values. We have pursued the second option, using the results from the GGT (profile AA' in Fig. 2) and the INDEPTH (BB' in Fig. 2) transects. The Moho was seen by active seismic sounding only in the first third of the INDEPTH profile (Nelson et al., 1996) and was found to be located at the depth of about 75 km. To the north, the position of the Moho is constrained by receiver function determinations from the broad band earthquake data. These indicate that the Moho lies between depths of about 70 and 80 km along the length of the survey (Kind et al., 1996; Makovsky et al., 1996). Apart from a fixed bias due to the conversion of time delays to depths, the uncertainty in the determination of the Moho is of the order of ± 5 km. This uncertainty is conservative for the seismic investigations by fan-profiling (GGT transect), and is adequate for the depth estimation obtained from wide-angle observation of P -to- S -wave conversion (Nelson et al., 1996). The seismic Moho depths according to the two transects INDEPTH (dots) and GGT (crosses and diamonds, referring to the papers of Wu et al. (1991a) and Hirn et al. (1984), respectively) are plotted in Fig. 6. The continuous line shows the gravimetric Moho for different pairs of density contrast across the Moho and reference depth (d), the density varying between 0.3 and 0.4×10^3 kg/m³ and the reference depth between 30 and 40 km.

Apart from local discrepancies, the range of possible models is of 30 km depth with density $\rho = 0.3\text{--}0.4 \times 10^3$ kg/m³, 35 km depth with density $\rho = 0.35\text{--}0.4 \times 10^3$ kg/m³, or 40 km depth and density $\rho = 0.4 \times 10^3$ kg/m³. The greatest discordance is between km-marks of 100 and 300 km along the profile with the values reported by Hirn et al. (1984). According to Hirn et al. (1984), just to the north of the high Himalayas a disruption of the Moho is observed, resulting in a Moho step. This observation was not confirmed by the INDEPTH- investigations. The minimum and maximum crustal depths, and the rms (root mean square) of the gravity residual are given in Table 1, for iteration steps 1–4. The values in the table pertain to the reference depth equal to 35 km and the density contrast of 0.4×10^3 kg/m³. It can be seen that already at the third iteration, no considerable reduction in the residual is achieved. For reference, the initial gravity standard deviation from the mean is 207 mgal.

In Fig. 6 the observed Bouguer anomaly and the topography along the profile are graphed. For orientation the intersections with the main sutures are added on the topography (YZ = Yarlung Zangbo, BN = Bangong Nujiang, JS = Jinsha, KL = Kunlun). Some interesting features emerge regarding our Moho model, as obtained from the gravity inversion: the sharp increase of topography in the south is reflected by a steep deepening of the Moho. The greatest

Moho depth is shifted to the north with respect to the highest topography (high Himalayas). The Moho shows an upwelling near Central Tibet, which resulted also from the gravity inversion of Jin Yu et al. (1994) and Jin Yu et al. (1996). The alternation of a Moho trough and high is observed to the north of this upwelling, before the Moho reaches shallow values in Northern Tibet.

The results for the 3D Moho undulations obtained from the gravity inversion are graphed in

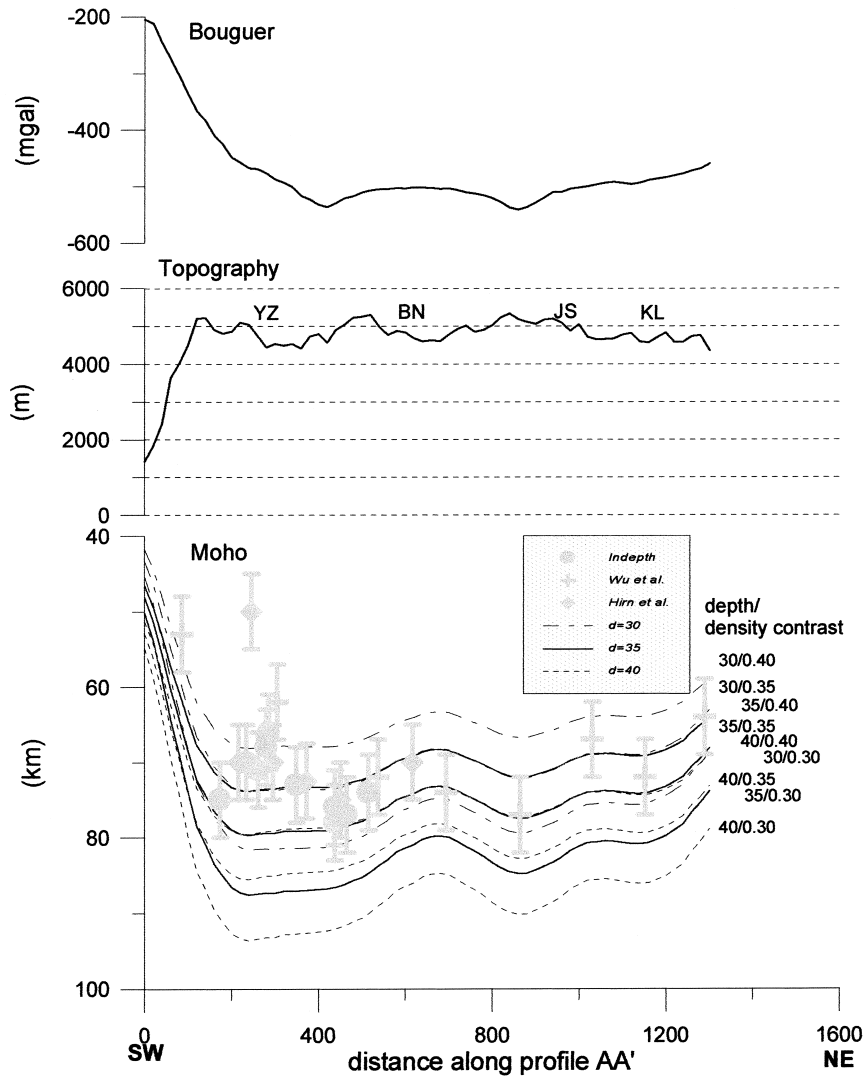


Fig. 6. The Bouguer, topography and the seismic and gravity Moho along profile AA'. The intersection with main suture lines is indicated by YZ (Yarlung Zangbo), BN (Bangong Nujiang), JS (Jinsha) and KL (Kunlun). The seismic Moho is shown according to the different sources as dots (Nelson et al., 1996), diamonds (Hirn et al., 1984) and crosses (Wu et al., 1991a). The gravity Moho is shown for different couples of the reference depth and the density contrast.

Table 1

Summary of the four iterations of the gravity inversion. Minimum and maximum depth of the Moho and rms of the gravity residual. Reference depth set to 35 km, density contrast equal to $0.4 \times 10^3 \text{ kg/m}^3$

Iteration	Max-root (km)	Min-root (km)	rms residual (mgal)
1	72.0	39.9	28.0
2	78.1	38.6	21.4
3	81.1	37.1	20.7
4	83.1	35.4	20.7

Fig. 7, the inversion having been made with the Moho reference depth of 35 km and the density contrast of $0.4 \times 10^3 \text{ kg/m}^3$. Due to the range of acceptable couples of reference depth and density contrast, the uncertainty on the Moho model is a systematic shift of at least ± 5 km.

The deepest Moho is found along the southern, western and northern margin of the Tibet plateau, with values which reach 80 km depth. The shallowest values of Central Tibet are found along most of the Bangong Nuijiang suture, with depths ranging between 70 and 65 km. Shallow Moho depths are also found beneath the Bayan Har-Songpan block in the north-eastern part of Tibet, where the Moho rises to 60 km depth. Most of the Tarim basin reveals Moho depths of 45–50 km, only the central part having more shallow values between 35 and 40 km.

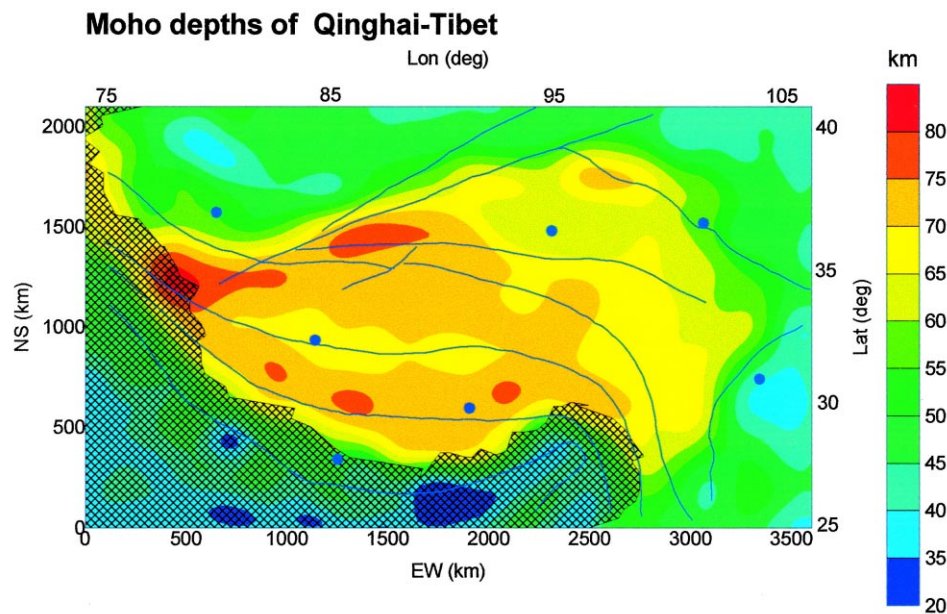


Fig. 7. Moho depths obtained from the gravity inversion according to the reference depth of 35 km and the density contrast of $0.4 \times 10^3 \text{ kg/m}^3$.

5. Percentage of isostatic compensation

The Moho depths we have calculated from gravity inversion have been obtained without taking into account the topography or any isostatic hypothesis. We now intend to compare the gravity Moho with the Moho expected from isostasy, or equivalently to study the amount of compensation according to an isostatic model. The isostatic compensation is defined (Bott, 1971) as the percentage of the observed crustal root with respect to the expected isostatic root.

It has been shown that at long wavelengths the Moho predicted with isostatic lithospheric flexure models converges to the isostatic root according to Airy (Turcotte and Schubert, 1982). It is therefore justified to consider the isostatic Airy model, when limiting the analysis to long wavelengths. We thus apply a low-pass filter to the gridded topography, using the filter described in the previous paragraphs and characterized by the 200 km cut-off wavelength. The coefficients necessary in the Airy model are obtained from regression analysis. The regression is extended over the entire studied area, except for the portions for which the dense gravity covering was not available (hatched area in Fig. 3). The Fig. 8 shows the scatterplot of the gravity Moho depths and the topography. With m the isostatic Moho (in km), and t the topography (in m), the regression gives us the following Airy-relation:

$$m = 36.4 + 0.0069t \quad (3)$$

It is seen that the reference depth we obtained from anchoring the gravity inversion with the seismic data (35 km) is close to the zero-topography Moho depth in the Airy isostatic compensation model (36 km). Assuming a density contrast of $0.4 \times 10^3 \text{ kg/m}^3$ across the Moho, the linear coefficient (0.0069) leads to a crustal density of $2.76 \times 10^3 \text{ kg/m}^3$. The crustal roots are obtained by subtracting the zero-topography crustal thickness (36.4 km) from the gravity and isostatic Moho depths, respectively.

A compensation greater than 100% is equivalent to over-compensation and is obtained when the gravity Moho is deeper than the isostatic Moho depth. An undercompensation is obtained when the gravity Moho is shallower than the isostatic Moho.

In Fig. 9, the amount of isostatic compensation in Tibet is shown, obtained from the ratio of the gravity crustal root and the expected Airy isostatic root. As before, the hatched region

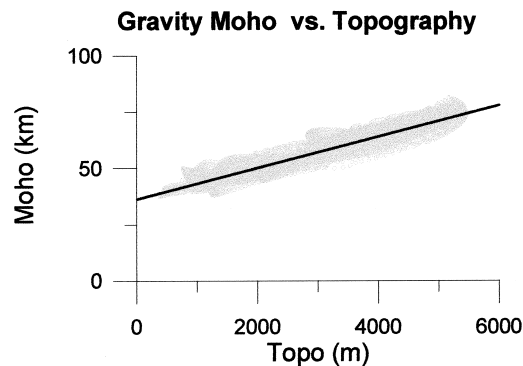


Fig. 8. Scatterplot of the gravity Moho (km) and the lowpass filtered topography (m) with the regression line.

marks the area for which we do not have the detailed gravity data. The main faults are shown as blue continuous lines, and dots give locations of major towns. The black heavy line marks the extension of the Tibet plateau, and shows the line for which topography exceeds 3000 m. This follows the demarcation of the Tibet plateau as introduced by Fielding et al. (1994). Most of Tibet is isostatically compensated, the compensation being between 90% and 110%. Along the margins of Tibet, the topography is over- or under-compensated. All of the eastern part of the Tarim basin has a crustal root considerably thicker than expected from isostasy, leading to an extended region of over-compensation. Remarkable is also the localized area of over-compensation, which is found in correspondence to the topographic depression in North-Eastern Tibet, the Qaidam basin. Conclusively, we may observe that most of the Tibet margin is characterized by a coupled over- and under-compensation across the margin, the over-compensation being localized inside Tibet, the under-compensation outside of Tibet.

6. Discussion and conclusions

In the present study existing gravity data are inverted in order to obtain a 3D model of the Moho undulations throughout the Tibet plateau and the neighbouring regions to the north and east. The inversion method has been tested on synthetic and real cases (Alps, Kohistan) for 2.5D and 3D modeling, and has shown to furnish reliable results (Braitenberg et al., 1997; Braitenberg and Drigo, 1998; Braitenberg and Zadro, 1999). A previous study regarding the spectral analysis of the gravity field over Tibet (Jin Yu et al., 1994) has shown that the field at spatial frequencies higher than 1/150 per km is due to sources in the upper crust, and that the

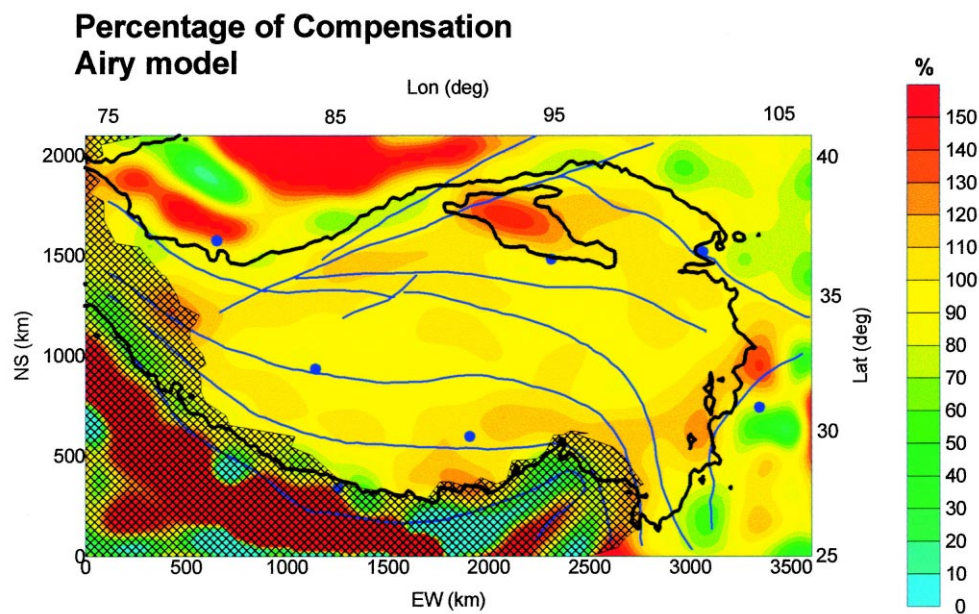


Fig. 9. Level of isostatic compensation at long wavelengths ($\gamma > 200$ km) according to the Airy model.

variations at lower frequencies are due to sources seated deeper. This result is a statistical evaluation based on the method of Spector and Grant (1970). At present the lack of information on the finer structure of overall Tibet makes this the only method to separate the Moho gravity effect from the total observed field. We use this result in that our inversion considers the gravity field at frequencies lower than 1/200 per km. The very long wavelength gravity contribution does not enter the inversion process, as it is taken off by a model of lithospheric thickening which bases on the seismologic lithosphere model (Zhou et al., 1991).

The inversion method integrates gravity data with results from deep seismic sounding: the Moho from deep seismic sounding is used to anchor the gravity Moho. For Tibet this was possible along the Yadong Golmud profile, where the results from Sino–Chinese (Hirn et al., 1984) and international efforts (Nelson et al., 1996) were integrated. The seismic information allows to “anchor” the gravity Moho with an uncertainty of about ± 5 km. We must therefore allow for a systematic upward or downward shift of about this amount (5 km) in the inverted gravity Moho. This tolerance may be reduced in the future, when more seismic investigations become available.

The gravity inversion is made under the assumption that the density contrast across the Moho is constant. The presence of a lateral variation of the density contrast would provoke a modification of the Moho undulation, nearly proportional to the variation in density. The existence of a lower density contrast, would lead to a local Moho deepening, for example. Presently, it is though not feasible to create a different density model, due to the lack of constraints.

Crossing Tibet along an E–W profile one observes an essentially flat Moho, in the contrary to a profile which cuts Tibet along its shorter side, when the presence of an undulation of several km amplitude is observed. The wavelength of the oscillation, calculated as the peak to peak and trough to trough distance varies between 200 and 460 km. The Moho oscillation across the plate could be connected to the buckling of the crust in response to the compression exercised by the Indian to Eurasian plate collision (Jin Yu et al., 1994). For a further discussion of the results along profiles crossing the plateau see also the complementary paper by Braitenberg et al. (1999).

We study the gravity Moho in terms of Airy isostatic compensation at long wavelengths. The compensation is calculated in terms of the percentage of the gravity crustal root with respect to the Airy root. Most of Tibet is found to be compensated at a level of 90–110%. An exception is given by the Qaidam basin, a topographic depression in North-Eastern Tibet which does not have a counterpart in the Moho topography, leading to an overcompensated crust. Similarly also the Tarim basin is overcompensated (150%), although the Moho is a lot more shallow than under Central Tibet. The border of Tibet is characterized by a coupled over/under-compensation. This is comparable to the situation in mountain ranges as for instance the Eastern Alps, where the axis of maximum crustal depth is shifted northwards with respect to the topographic crest (Braitenberg et al., 1997). An explanation could be the drag exerted at the base of the crust by the converging lithosphere, which could lead to a shift oriented towards the direction of the drag.

We may conclude that the inversion has furnished a reliable long wavelength model of the Moho undulations. Our model reproduces the Moho undulations from a gravimetric and deep seismic sounding standpoint, and is independent from assumptions regarding the dynamics

involved. It can therefore be used as important independent input for future dynamic models which aim to explain the Indian–Eurasian collision belt. Our considerations on isostasy over Tibet have shown that at long wavelengths over most of Central Tibet isostatic equilibrium is satisfied. It may be concluded that the present uplift of Tibet is not due to isostatic adjustments at crustal level. One possible candidate to cause the uplift is the underplating of Tibet by the Indian plate. Another mechanism is ascribable to a process of folding and shortening of the Tibetan crust, due to a compression exerted by the Indian–Eurasian collision, and a consequent vertical expansion of the crustal material giving way in the direction of least resistance. It should be tested in the future whether the areas of isostatic over-compensation, as the Qaidam and the Tarim basins, are distinguished by increased uplift rates and/or other signs of increased instability with respect to the remainder of the plateau.

Acknowledgements

The inversion was carried out during a stay of CB at Wuhan, profiting from a grant financed by the Italian CNR— Chinese Academy of Sciences agreement of cooperation. In the frame of this agreement successively a stay was granted to JF and HSH at Trieste University, during which the work was further discussed. Prof. W. Jacoby and Prof. E. Kissling are thanked for constructive reviews. The work was partly financed by CNR grants CT 98.00159 and CT97.00121.

References

- Bott, M.H.P., 1971. *The Interior of the Earth*. Edward Arnold, London, pp. 1–316.
- Braitenberg, C., Pettenati, F., Zadro, M., 1997. Spectral and classical methods in the evaluation of Moho undulations from gravity data: the N-E Italian Alps and isostasy. *J. Geodynamics* 23, 5–22.
- Braitenberg, C., Drigo, R., 1997. A crustal model from gravity inversion in Karakorum. In: *Proceedings of the Int. Symp. on Current Crustal Movement and Hazard Reduction in East Asia and South-East Asia*, November 4–7, Wuhan, 325–341.
- Braitenberg, C., Zadro, M., 1999. Iterative 3D gravity inversion with integration of seismologic data. *Proceedings of the 2nd Joint Meeting IAG and IgeC*, 7–12 September, 1998, Trieste, Italy. *Bollettino di Geofisica Teorica ed Applicata* 40, (2).
- Braitenberg, C., Zadro, M., Fang, J., Wang, Y., Hsu, H.T., 1999. Gravity inversion Qinghai–Tibet plateau. *Physics and Chemistry of the Earth* (in press).
- Brown, L.D., Zhao, W., Nelson, K.D., Hauck, M., Alsdorf, D., Ross, A., Cogan, M., Claek, M., Liu, X., Chen, J., 1996. Bright spots structure, and magmatism in southern Tibet from INDEPTH seismic reflection profiling. *Science* 274, 1688–1690.
- Chen, L., Booker, J.R., Jones, A.G., Wu, N., Unsworth, M.J., Wenbo, W., Tan, H., 1996. Electrically conductive crust in southern Tibet from INDEPTH magnetotelluric surveying. *Science* 274, 1694–1696.
- Chengfa, C., Nansheng, C., Coward, M.P., Wanming, D., Dewey, J.F., Gansser, A., Harris, N.B.W., Chengwei, J., Kidd, W.S.F., Leeder, M.R., Huan, Li, Jinlu, L., Chengije, L., Houjun, M., Molnar, P., Yun, Pan, Yusheng, Pan, Pearce, J.A., Shackleton, R.M., Smith, A.B., Yiyin, Sun, Ward, M., Watts, D.R., Juntao, Xu, Ronghua, Xu, Jixiang, Yin, Yuquan, Zhang, 1985. Preliminary conclusions of the Royal Society and Academia Sinica 1985 geotraverse of Tibet. *Nature* 323, 501–507.
- Fielding, E., Isacks, B., Baranzangi, M., Duncan, C., 1994. How flat is Tibet? *Geology* 22, 163–167.

- Hirn, A., Necessian, A., Sapin, M., Jobert, G., Xin, X.Z., Yuan, G.E., Yuan, L.D., Wen Teng, Ji, 1984. Lhasa block and bordering sutures — a continuation of a 500 km Moho traverse through Tibet. *Nature* 307, 25–27.
- Hsu, H.T., Jiang, F., 1995. Gravity variation in Lhasa, Qinghai–Xizang plateau. Publication dedicated to Erwin Groten on the occasion of his 60th anniversary, Munchen, pp. 62–67.
- Hsu, H.T., Lu, Yang., 1995. The regional geopotential model in China. *Bollettino di geodesia e Scienze Affini* LIV (N2), 161–175.
- Jackson, M., Bilham, R., 1994. Constraints on Himalayan deformation inferred from vertical velocity fields in Nepal and Tibet. *J. Geoph. Res* 99 (B7), 13897–13912.
- Jiang, F.-Z., Zhang, C.-J., Ni, Z.-H., Liu, Y.-P., 1989. The isostatic field of Qinghai–Xizang plateau and non-tide gravity measurement. *Chinese Journal of Geophysics* 32, 375–380.
- Jin, Yu., McNutt, M., Zhu, Yongsheng, 1994. Evidence from gravity and topography data for folding of Tibet. *Nature* 371, 669–674.
- Jin, Yu, McNutt, M., Zhu, Yongsheng, 1996. Mapping the descent of Indian and Eurasian plates beneath the Tibetan plateau from gravity anomalies. *Journ. Geoph. Res* 101 (B5), 11275–11290.
- Kind, R., Ni, J., Zhao, W., Wu, J., Yuan, X., Zhao, L., Sandvol, E., Reese, C., Nabelek, J., Hearn, T., 1996. Evidence from earthquake data for a partially molten crustal layer in southern Tibet. *Science* 274, 1692–1694.
- Lu, Yang, Houze, X., 1998. The study on high-resolution earth gravity model of 720 order, IGG97L. *Crustal Deformation and Earthquake* 1 (18(1)), 1–7 In Chinese.
- Ma, X.Y. (Ed.), 1989. *Lithospheric Dynamics Atlas of China*. China Cartographic, Beijing.
- Makovsky, Y., Klemperer, Ratschbacher, L., Brown, L., Li, M., Zhao, W., Meng, Fanle, 1996. INDEPTH wide-angle reflection observation of *P*-wave-to-*S*-wave conversion from crustal bright spots in Tibet. *Science* 274, 1690–1691.
- Meng, Lingshun, Gao, Rui, et al., 1992. Yadong–Golmud GGT Gravity Survey and the Lithosphere Structure in Qinghai–Tibet Plateau. *Geological*, Beijing (in Chinese).
- Molnar, P., 1990. A review of the seismicity and rates of active underthrusting and deformation at the Himalaya. *J. Himalayan Geol* 1, 131–154.
- Nagy, D., 1966. The gravitational attraction of a right rectangular prism. *Geophysics* XXX, 362–371.
- Nelson, K.D., Wenjin, Zhao., Brown, L.D., Kuo, J., Jinkai, Che, Xianwen, Liu., Klemperer, S.L., Makovsky, Y., Meissner, R., Mechie, J., Kind, R., Wenzel, F., Ni, J., Nabelek, J., Chen, Leshou, Handong, Tan, Wenbo, Wei, Jones, A.G., Booker, J., Unsworth, M., Kidd, W.S.F., Hauck, M., Changde, Wu, Sandvol, E., Edwards, M., 1996. Partially molten middle crust beneath southern Tibet: synthesis of project INDEPTH results. *Science* 274 (6), 1684–1688.
- Parker, R.L., 1972. The rapid calculation of potential anomalies. *Geophys. J. R. Astr. Soc* 31, 447–455.
- Spector, A., Grant, F.S., 1970. Statistical models for interpreting aeromagnetic data. *Geophysics* 35, 293–302.
- Sun, W., 1989. Bouguer Gravity Anomaly Map of the P.R. of China. Chinese Academy of Geoexploration of Geoexploration, Beijing.
- Turcotte, D., Schubert, G., 1982. *Geodynamics*. In: *Applications of Continuum Physics to Geological Problems*. Wiley, New York, pp. 1–450.
- Wang, Y., Hsu, H.T., 1996. The variations of lithospheric flexural strength and isostatic compensation mechanisms beneath the continent of China and actaisostatic compensation mechanisms beneath the continent of China and its vicinity. *Acta Geophysica Sinica*. 39 (Suppl. C), (in Chinese).
- Wu Gong, Jian., Gao, Rui., Yu, Qin-Fan., Cheng, Qing-Yun., Meng, Ling-Shun., Dong, Xue-Bin., Chui, Zuo-Zhuo., Yin, Zhuo-Xun., Shen, Xian-Jie., Zhou, Xian-Jie., Chui, Zuo-Zhou., Yin, Zhou-Xun., Shen, Xian-Jie., Zhou, Yao-Xiu. (1991). Integrated investigations of the Qinghai-Tibet plateau along the Yadong Golmud geoscience transect. *Acta Geophysica Sinica*. 34 (5), 552–562, (in Chinese).
- Wu, G.J., Xiao, X.C., Li, T.D., 1991. Yadong to Golmud Transect: Qinghai-Tibetan Plateau China, *Global Geosci. Transects*, 3, AGU, Washington D.C.
- Xiong, S., 1985. Crust depth and Moho undulations in Tibetan plateau. *Acta Geophysica Sinica* 28 (2), 16–27.
- Zadro, M., Braitenberg, C., 1997. Spectral methods in gravity inversion: the geopotential field and its derivatives. *Annali di Geofisica* XL (5), 1433–1443.
- Zeng, R.-S., Sun, W.-G., 1993. Seismicity and focal mechanism in Tibetan plateau and its implications to lithospheric flow. *Acta Seismologica Sinica* 6, 261–287.

- Zhao, Wenjin., Nelson, K.D., Project INDEPTH Team, 1993. Deep seismic reflection evidence for continental underthrusting beneath southern Tibet. *Nature* 366, 557–559.
- Zhou, B., Zhu, J.S., Chun, K.Y., 1991. Three dimensional shear wave velocity structure beneath Qinghai–Tibet and its adjacent area. *Acta Geophysica* 34 (4), 426–441.